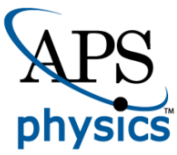

Tuning Edge States in Strained-Layer InAs/GaInSb Quantum Spin Hall Insulators

Lingjie Du, Tingxin Li, Wenkai Lou, Xingjun Wu, Xiaoxue Liu, Zhongdong Han, Chi Zhang, Gerard Sullivan, Amal Ikhlassi, Kai Chang, and Rui-Rui Du

Phys. Rev. Lett. **119**, 056803 — Published 3 August 2017

DOI: 10.1103/PhysRevLett.119.056803

Tuning Edge States in Strained-Layer InAs/GaInSb Quantum Spin Hall Insulators

Lingjie Du[1†], Tingxin Li[1, 2†], Wenkai Lou[3], Xingjun Wu[2], Xiaoxue Liu[2], Zhongdong Han[2], Chi Zhang[2,4], Gerard Sullivan[5], Amal Ikhlassi[5], Kai Chang[3], Rui-Rui Du[1,2,4*]

[1]*Department of Physics and Astronomy, Rice University, Houston, Texas 77251-1892, USA*

[2]*International Center for Quantum Materials, School of Physics, Peking University, Beijing 100871, China*

[3]*SKLSM, Institute of Semiconductors, Chinese Academy of Sciences, Beijing 100083, China*

[4]*Collaborative Innovation Center of Quantum Matter, Beijing 100871, China*

[5]*Teledyne Scientific and Imaging, Thousand Oaks, California 91603, USA*

[†] These authors contributed equally to this work.

[*] Corresponding author: Rui-Rui Du at rrd@rice.edu

Abstract

We report on a class of quantum spin Hall insulators (QSHIs) in strained-layer InAs/GaInSb quantum wells, in which the bulk gaps are enhanced by up to five folds as compared to the binary InAs/GaSb QSHI. Remarkably, with consequently increasing edge velocity, the edge conductance at zero and applied magnetic fields manifests time reversal symmetry (TRS) -protected properties consistent with Z_2 topological insulator. The InAs/GaInSb bilayers offer a much sought-after platform for future studies and applications of the QSHI. .

Introduction TRS protected quantum spin Hall effect (QSHE) is predicted in a two-dimensional topological insulator [1-4] with a topological number Z_2. The transport evidence for QSHE was first observed [5] in HgTe/CdTe quantum well (QW) with its edge conductance quantized to the theoretical value. To date the leading materials systems are made of semiconductor QWs, *i.e.*, HgTe/CdTe QW and inverted InAs/GaSb QWs; both are described by the Bernevig-Hughes-Zhang model [4]. In InAs/GaSb QWs, wave-function hybridization between InAs and GaSb layers dominates the bulk and opens a minigap Δ [6], while a Kramer's pair of spin-momentum-locked edge states emerges on the device perimeters [7]. Relevant experiments are reported in refs [8-17]. The charge transport in helical edges is dissipationless, owning to the notion that the helical property prevents charge backscattering. On the other hand, theories [18-20] taking into account electron-electron interactions and correlations suggest that certain many-body scattering processes may exist, which should lead to dissipation.

In the inverted InAs/GaSb bilayer system, the ground electron sub-band in InAs well and the ground hole sub-band in GaSb well cross at certain wave-vectors k_{cross}. Spatially separated electrons and holes are strongly coupled at this crossing point due to the tunneling between the two wells; consequently, a hybridization gap Δ is opened at k_{cross}, which is the bulk gap of the QSHI. The density of the charge neutral point (CNP) in the inverted regime is referred to as $n_{cross} = k_{cross}^2 / 2\pi$. The degree of band inversion can be tuned by QW widths and gate voltages [6, 8-16], and it has dramatic influences on the bulk transport properties. In the deeply inverted regime where typically n_{cross} above $\sim 2 \times 10^{11}$ cm^{-2}, there always exist considerable residual states in the hybridization gap thus the bulk of InAs/GaSb QWs is not truly insulating [8,9,12,13], which limits the studies and applications of QSHE.

On the other hand, in the shallowly inverted regime (n_{cross} below $\sim 1 \times 10^{11}$ cm^{-2}), the bulk is insulating to a high degree and quantized helical edge conductance plateaus were observed [10,15]. Surprisingly, the quantized conductance plateaus persist under external magnetic fields, in contrast with the theoretical expectations for TRS protected helical edge states [10]. On a general ground, Coulomb interactions of electron-hole pairs dominate over hybridization effects in such a dilute limit [21], leading to the possibility of a 2D excitonic ground state [21-23]. Moreover, here the edge Fermi velocity $v_F \sim \Delta / 2\hbar k_{cross}$ is unusually small, in the range of $\sim 2 \times 10^4$ ms^{-1} to $\sim 5 \times 10^4$ ms^{-1}, indicating that the edge states are in a strongly interacting regime [18-20,24]. Overall, while the quantized edge transport has been observed in micrometer size samples of shallowly inverted InAs/GaSb, the resilience to

external magnetic field and the observed length dependence in long samples are not account for by single-particle model. From an experimental perspective, it is much desirable to develop a plain vanilla QSHI with properties dominated by single-particle physics. Ideally, to some degree the interaction effects may be set in by tuning experimental parameters such as v_F.

In this Letter, we report on a QSHI in strained-layer InAs/GaInSb QWs, which clearly manifests TRS protected properties. Due to the band structural changes from strain effect, QWs can be made narrower, leading to stronger overlaps between electron and hole wave functions. This effect results in insulating hybridization gaps at low temperatures even when the n_{cross} is larger than 3×10^{11} cm^{-2}. In addition, the helical edge conductance decreases under either perpendicular or in-plane magnetic fields, indicating the opening of mass gaps in the edge states. Remarkably, we found that the edge conductance and the magnetic response are correlated with v_F, which could be well controlled by lattice strain and the gate voltages.

Strain effect in InAs/GaInSb Strain-engineering is a common way to modify the band structure and physical properties for semiconductor materials, and recently for topological materials [25,26]. Specific to InAs/GaInSb system, strained-layer InAs/$Ga_{1-x}In_xSb$ superlattice (SL) infrared detectors were proposed [27] by Smith and Maihiot in 1987. By alloying GaSb (lattice constant about 6.1 Å) with InSb (6.4 Å), because of the strain in the growth plane, the energy of the conduction band (CB) in InAs shift downward while the energy level of valence band (VB) in GaInSb splits into heavy hole (HH) level and light hole (LL) level, respectively, where the energy of the HH level is higher than the original top VB in GaSb. As a result, to reach a fixed energy band gap, the layers of InAs/GaInSb SL are made narrower than InAs/GaSb SL thereby increasing the optical absorption efficiency. Such strain-engineering has led to the invention of high-performance long-wave length SL infrared detectors [28].

Similar physics idea may guide the construction of a large-gap QSHI. Based on the strain effects described above, we can reach the same inverted band structure with narrower QWs in strained-layer InAs/GaInSb, comparing to unstrained InAs/GaSb. The hybridization-induced gap should increase in such narrower QWs primarily due to the enhanced overlap of electron and hole wavefunctions. In addition, due to the energy splitting of the HH and LH in GaInSb, the Fermi surface of electrons would better match with the Fermi surface of holes, which also help to reduce the residual non-hybridized carriers.

Fig. 1(a)-1(c) shows calculated band structure of strained InAs/$Ga_{1-x}In_xSb$ QWs with different indium concentrations (x = 0.20, 0.25, 0.32) by 8-band Kane model. The results indicate that a ~ 20 meV hybridization gap could be achieved in the [100] direction in InAs/$Ga_{0.68}In_{0.32}Sb$ QWs, which is about five-fold enhancement from the value ~ 4 meV in unstrained InAs/GaSb QWs. Depending on gating conditions, measured bulk gap is around this value. The wafers we used for the present experiment was grown by molecular beam epitaxy (MBE). As an example, the structure of a 9.5 nm InAs/ 4 nm $Ga_{0.75}In_{0.25}Sb$ QWs is shown in Fig. 1(e). Fig. 1(f) is a transmission electron microscope (TEM) photograph of an InAs/$Ga_{0.68}In_{0.32}Sb$ wafer; it shows that the crystalline structure remains coherent across the heterostructure interfaces regardless of ~ 1.5 % in-plane strain.

Transport properties of bulk states in strained-layer InAs/GaInSb QWs In order to directly measure the bulk conductance, we fabricate dual-gated Corbino devices. In this case, the edge conductance is shunted and has no contribution to the signals. Fig. 2(a)&2(c), and 2(b)&2(d) shows the traces of the conductivity versus front-gate voltage V_{front} measured from a Corbino device made by the InAs/$Ga_{0.75}In_{0.25}Sb$ QWs at temperature T ~ 20 mK, with back gate voltage V_{back} = 0 V and V_{back} = 4 V, respectively. At the CNP, the conductivity show dips, indicating the entrance into an energy gap. For more positive V_{back}, the bulk band becomes more inverted, resulting in a less insulating bulk. Nevertheless, the bulk conductivity is still negligible at low temperature, about 100 MΩ per square at 20 mK for the V_{back} = 0 V case, and about 25 MΩ per square at 20 mK for the V_{back} = 4 V case. Note that even for the V_{back} = 0 V case, the n_{cross} value of this wafer is larger than 2 × 10^{11} cm^{-2}, corresponding to the modestly deep-inverted regime. Hybridization gaps with residual conductivity have been commonly reported in deeply inverted InAs/GaSb QWs [6,8,12,13]; this is the first time that a substantially insulating hybridization gap is observed at low temperature.

Electron-hole hybridization are most favored when the Fermi momentum of electrons k^e_F and holes k^h_F are equal. Under in-plane magnetic field $B_{//}$, applied along x axis of the example, Lorenz force gives tunneling carriers additional momentum along y axis, resulting in a relative shift of band dispersions $\Delta k_y = -eB \Delta \langle z \rangle / h$, (tunneling distance $\Delta \langle z \rangle$ is limited by one-half thickness of the QWs). Consequently, carrier hybridization is suppressed due to momentum-mismatch, rendering the QWs as a bilayer-semimetal. As shown in Fig. 2(a) and 2(b), the gap at CNP is gradually closed with an increasing $B_{//}$. Similar behaviors have also been observed in the InAs/$Ga_{0.80}In_{0.20}Sb$ QWs (Fig 2(e)) and InAs/$Ga_{0.68}In_{0.32}Sb$ QWs (Fig

2(f)). This observation agrees with the behavior of a hybridization gap under in-plane magnetic field, but in contrast to the behavior of the insulating gap observed in a shallowly-inverted InAs/GaSb QW [23], where the bulk gap does not show sign of closing in a very high field. Under perpendicular magnetic field $B_{\perp}$, the bulk becomes more insulating due to localization effects, as shown in Fig. 2(c) and 2(d).

Information of the bulk gaps can be further obtained from temperature dependent conductance. Fig. 2(g) shows the Arrhenius plots of Corbino devices made of strained-layer InAs/$Ga_{1-x}In_xSb$ QWs (x = 0.20, 0.25, and 0.32) and the shallowly inverted InAs/GaSb QWs (data adapted from Ref. 10 at B = 0 T). It lacks the exponential dependences in the tail regime for the strained layer wafers; the transport there is more like variable-range hopping. Indeed, this is a characteristic feature for transport in hybridization gap, as discussed in ref. 8. At higher temperatures, the hybridization gap values can be estimated by fitting the Arrhenius plots, which is ~ 66 K for the shallowly inverted InAs/GaSb QWs, ~ 120 K for the InAs/$Ga_{0.80}In_{0.20}Sb$ QWs, ~ 130 K for the InAs/$Ga_{0.75}In_{0.25}Sb$ QWs, and ~ 250 K for the InAs/$Ga_{0.68}In_{0.32}Sb$ QWs. Overall, larger hybridization gaps have been achieved by strain-engineering, in reasonable agreement with the calculations.

Controllable helical edge states with long characteristic length We now turn to the helical edge properties of strained-layer InAs/$Ga_{0.75}In_{0.25}Sb$ QWs. Fig. 3(a) shows the longitudinal resistance R_{xx}-V_{front} traces of a 100 μm × 50 μm Hall bar device with various V_{back} at T ~ 20 mK. Here the measured R_{xx} is solely resulted from the edge channels, since the bulk is fully insulating at such low T. At V_{back} = 0 V, the resistance peak is about 115 kΩ, corresponding to a characteristic length λ_{φ} (refers to a length scale at which dissipationless edge transport breaks down and counter propagating spin-up and spin-down channels equilibrate) about 11 μm. The λ_{φ} of different devices made by this wafer typically range from ~ 5 μm to 10 μm, significantly longer than those in previous studies [5,10] of the QSHI. Remarkably, the λ_{φ} can be tuned by gate: as shown in Fig. 3(a) the resistance peak values gradually decreases with decreasing V_{back} (namely, less inverted), indicating that the λ_{φ} increase from ~ 6 μm at V_{back} = 4 V to ~ 11 μm at V_{back} = 0 V. (Note for this device the backgate bias was limited within 4V and 0V). The insets of Fig. 3(a) illustrate the λ_{φ} and the n_{cross} (deduced from magneto-transport data) versus V_{back}.

According to the definition of characteristic length, if the device edge length is shorter than λ_{φ}, the edge, conductance measured should be quantized to $2e^2/h$. This is indeed confirmed in a Hall bar device of length 10 μm, as shown in Fig. 3(b). As the λ_{φ} is being

tuned from 6 μm to 11 μm, the R_{xx} decreases, and finally reaches a plateau of 12.9 kΩ with a reasonable accuracy.

A plausible explanation for above data is related to the interaction effects [18-20] in the helical edge state. At more positive V_{back}, the bulk band becomes more inverted hence a larger k_{cross} and a roughly constant Δ [7]; overall this would lead to a smaller Fermi velocity $v_F \sim \Delta / 2\hbar k_{cross}$ of the helical edge states, resulting in more prominent interaction effects for the edge states. The backscattering processes would enhance when the electron-electron interactions become stronger, thus the helical edge states exhibit a shorter characteristic length in the more inverted case.

TRS protected helical edge states In general, applying magnetic field will break the TRS and open a gap in the helical edge states. 1D massless Dirac fermion could be tuned into 1D massive fermion allowing for backscattering, thereby the helical edge resistance will increase. However, in previous studies [10] of shallowly-inverted InAs/GaSb QWs, the quantized conductance plateaus are found to persist under external magnetic fields, in contrast with the theoretical expectations for TRS protected helical edge states.

Remarkably, for all devices made by strained-layer InAs/GaInSb QWs, the helical edge conductance show clear magnetic field dependence. Specifically, for a 3 μm × 1.5 μm Hall bar device made by the InAs/$Ga_{0.75}In_{0.25}Sb$ QWs, a quantized plateau of $h/2e^2$ has been observed at zero magnetic field, as shown in Fig. 4(a) and 4(b). Under a perpendicular magnetic field, as shown in Fig. 4(a), the plateau values (R_{CNP}) increase at first ($B_\perp$ below 5 T) due to TRS breaking, then decrease at higher $B_\perp$, indicating the edge states undergoing a transition from helical edge states to chiral edge states [10]. Similar behaviors were observed for the longer sample of 100 μm × 50 μm Hall bar, as shown in Fig. 4(c) and 4(d).

The response to an in-plane field $B_{//}$ shows an interesting behavior. Under a small $B_{//}$ up to 3 T (Fig. 4(b)), the measured resistance of the 3 μm × 1.5 μm Hall bar increases due to TRS breaking. For $B_{//}$ above 3 T, we observed that the sample resistance decreases with $B_{//}$, primarily because the bulk becomes conductive under higher $B_{//}$ (see Fig. S4 and S5 of Supplemental Material [29]).

Following comments are in order. 1) The helical edge states here should be described as a weakly interacting 1D helical liquid without axial spin symmetry, *i.e.*, spin S_z is momentum dependent [31]. Consequently, additional TRS-allowed inelastic scattering channels exist. Our data show, that an external magnetic field (either $B_\square$ or $B_{//}$, or in a combination of both) would cause the edge resistance R_{xx} to increase, qualitatively consistent with this spin texture

picture; 2) Maciejko *et al* [32] studied the combined effect of disorder and TRS breaking on QSH edge transport. They conclude that in the absence of TRS, the edge liquid is topologically equivalent to a spinless 1D quantum wire, and therefore subject to Anderson localization by disorder. We note that (refer to Fig. 4) under magnetic field the R_{xx} increases throughout the bulk gap, indicating bulk disorder may play a role in localization of the edge states [32]; and 3) It appears that the response of R_{xx} to a magnetic field correlates with λ_φ (hence with v_F). This can be seen in a 100 μm × 50 μm Hall bar under $B_{\square}$ = 1 T at V_{back} = 0 V (Fig. 4(c)) and V_{back} = 4 V (Fig. 4(d)) , where R_{xx} increases by 41% (32%) for λ_φ ~ 10.7 μm (6.8 μm), respectively.

Discussion on Luttinger parameter K One of the most attractive features of the strained-layer InAs/GaInSb system is the relatively large hybridization gap, and the gap size can be well controlled by the strain of the QWs. A larger hybridization gap leads to an increasing edge v_F . Electron-electron interaction effects in the helical edge can be parameterize by *K*, and *K* is strongly correlated with v_F and other factors such as screening from the environment [19,20]. In general, the helical Luttinger liquid has several fix points in the axis of *K*, namely, *K* = 1, *K* = 1/2, and *K* = 1/4. For helical edge states in (regular) InAs/GaSb QWs [24] assuming v_F ~ 5 × 10^4 ms^{-1}, we have determined *K* ~ 0.22, which is close to 1/4.

As for the strained-layer InAs/GaInSb system, if we adopt a hybridization gap ~ 20 meV, n_{cross} from (1 to 2) × 10^{11} cm^{-2}, QWs width ~ 12 nm, and screening length ~ 50 nm, the estimated v_F of helical edge states ranges then from (~ 1.9 to ~ 1.3) × 10^5 ms^{-1}, and consequently the *K* value from ~ 0.5 to ~ 0.43. Thus even without further refining, the present system should cover the range of 1/4 (strongly-interacting) through 1/2 (weakly-interacting) in Luttinger parameter.

Summary By strain-engineering, we have demonstrated for the first time a QSHI in InAs/GaInSb QWs clearly manifesting TRS protection, which shows a larger hybridization gap and longer characteristic length than existing QSHI systems. Moreover, the bulk is enough insulating at low temperatures and the edge characteristic length may be well controlled by the gates; data shows that the edge states can be gapped out by applying magnetic fields. Our findings not only move one step closer to the device and circuit applications of QSHI based on semiconductor technology, but also provide a nearly idea system for creating, detecting, and manipulating Majorana or parafermion bound states.

Acknowledgments We thank Carlo W. J. Beenakker, Xincheng Xie, and Shoucheng Zhang for helpful discussions. Work at Rice were funded by NSF Grants No. DMR-1508644 and Welch Foundation Grants No. C-1682, work at PKU were funded by NBRPC Grants No. 2014CB920901, work at IoS, CAS were funded by NSFC Grants No. 11434010 and NBRPC Grants No. 2015CB921503.

References

1. M. Z. Hasan and C. L. Kane, Colloquium: Topological insulators. *Rev. Mod. Phys.* **82**, 3045-3067 (2010).

2. X. L. Qi and S. C. Zhang, Topological insulator and superconductors. *Rev. Mod. Phys.* **83**, 1057-1110 (2011).

3. C. L. Kane and E. J. Mele, Z_2 topological order and the quantum spin Hall effect. *Phys. Rev. Lett.* **95**, 146802 (2005).

4. B. A. Bernevig, T. L. Hughes, and S. C. Zhang, Quantum spin Hall effect and topological phase transition in HgTe quantum wells. *Science* **314**, 1757-1761 (2006).

5. M. König, S. Wiedmann, C. Brüne, A. Roth, H. Buhmann, L. W. Molenkamp, X. L. Qi, and S. C. Zhang, Quantum spin Hall insulator state in HgTe quantum wells. *Science* **318**, 766-770 (2007).

6. M. J. Yang, C. H. Yang, B. R. Bennett, and B. V. Shanabrook, Evidence of a hybridization gap in "semimetallic" InAs/GaSb Systems. *Phys. Rev. Lett.* **78**, 4613-4616 (1997).

7. C. X. Liu, T. L. Hughes, X. L. Qi, K. Wang, and S. C. Zhang, Quantum spin Hall effect in inverted type-II semiconductors. *Phys. Rev. Lett.* **100**, 236601 (2008).

8. I. Knez, R. R. Du, and G. Sullivan, Finite conductivity in mesoscopic Hall bars of inverted InAs/GaSb quantum wells. *Phys. Rev. B* **81**, 201301(R) (2010).

9. I. Knez, R. R. Du, and G. Sullivan. Evidence for helical edge modes in inverted InAs/GaSb quantum wells. *Phys. Rev. Lett.* **107**, 136603 (2011).

10. L. Du, I. Knez, G. Sullivan, and R. R. Du, Robust helical edge transport in gated InAs/GaSb bilayers. *Phys. Rev. Lett.* **114**, 096802 (2015).

11. W. Pan, J. F. Klem, J. K. Kim, M. Thalakulam, M. J. Cich, and S. K. Lyo, Chaotic quantum transport near the charge neutrality point in inverted type-II InAs/GaSb field-effect transistors. *Appl. Phys. Lett.* **102**, 033504 (2013).

12. K. Suzuki, Y. Harada, K. Onomitsu, and K. Muraki, Gate-controlled semimetal-topological insulator transition in an InAs/GaSb heterostructure. *Phys. Rev. B* **91**, 245309 (2015).

13. S. Mueller, A. N. Pal, M. Karalic, T. Tschirky, C. Charpentier, W. Wegscheider, K. Ensslin, and T. Ihn, Nonlocal transport via edge states in InAs/GaSb coupled quantum wells. *Phys. Rev. B.* **92**, 081303(R) (2015).

14. F. Qu, A. J. A. Beukman, S. Nadj-Perge, M. Wimmer, B. M. Nguyen, W. Yi, J. Thorp, M. Sokolich, A. A. Kiselev, M. J. Manfra, C. M. Marcus, and L. P. Kouwenhoven, Electric and magnetic tuning between the trivial and topological phases in InAs/GaSb double quantum wells. *Phys. Rev. Lett.* **115**, 036803 (2015).

15. F. Couëdo, H. Irie, K. Suzuki, K. Onomitsu, and K. Muraki, Single-edge transport in an

InAs/GaSb quantum spin Hall insulator. *Phys. Rev. B.* **94**, 035301 (2016).

16. F. Nichele, H. J. Suominen, M. Kjaergaard, C. M. Marcus, E. Sajadi, J. A. Folk, F. Qu, A. J. A. Beukman, and F. K. de Vries, Edge transport in the trivial phase of InAs/GaSb. *New J. Phys.* **18**, 083005 (2016).

17. B. M. Nguyen, A. A. Kiselev, R. Noah, W. Yi, F. Qu, A. J. A. Beukman, F. K. de Vries, J. van Veen, S. Nadj-Perge, L. P. Kouwenhoven, M. Kjaergaard, H. J. Suominen, F. Nichele, C. M. Marcus, M. J. Manfra, and M. Sokolich, Decoupling Edge Versus Bulk Conductance in the Trivial Regime of an InAs/GaSb Double Quantum Well Using Corbino Ring Geometry. *Phys. Rev. Lett.* **117**, 077701 (2016).

18. C. Wu, B. A. Bernevig, and S. C. Zhang, Helical liquid and the edge of quantum spin Hall systems. *Phys. Rev. Lett.* **96**, 106401 (2006).

19. J. C. Y. Teo and C. L. Kane. Critical behavior of a point contact in a quantum spin Hall insulator. *Phys. Rev. B* **79**, 235321 (2009).

20. J. Maciejko, C. Liu, Y. Oreg, X. L. Qi, C. Wu, and S. C. Zhang. Kondo Effect in the Helical Edge Liquid of the Quantum Spin Hall State. *Phys. Rev. Lett.* **102**, 256803 (2009).

21. Y. Naveh and B. Laikhtman, Excitonic Instability and Electric-Field-Induced Phase Transition Towards a Two-Dimensional Exciton Condensate. *Phys. Rev. Lett.* **77**, 900 (1996).

22. D. I. Pikulin and T. Hyart, Interplay of Exciton Condensation and the Quantum Spin Hall Effect in InAs/GaSb Bilayers. *Phys. Rev. Lett.* **112**, 176403 (2014).

23. L. Du, W. Lou, K. Chang, G. Sullivan, and R. R. Du, Gate-tuned spontaneous exciton insulator in double-quantum wells. arXiv: 1508.04509.

24. T. Li, P. Wang, H. Fu, L. Du, K. A. Schreiber, X. Mu, X. Liu, G. Sullivan, G. A. Csáthy, X. Lin, and R. R. Du, Observation of a helical Luttinger liquid in InAs/GaSb quantum spin Hall edges. *Phys. Rev. Lett.* **115**, 136804 (2015).

25. E. Tang and L. Fu. Strain-induced partially flat band, helical snake states and interface superconductivity in topological crystalline insulators. *Nature Phys.* **10**, 964 (2014).

26. I. Zeljkovic, D. Walkup, B. A. Assaf, K. L. Scipioni, R. Sankar, F. Chou, and V. Madhavan. Strain engineering Dirac surface states in heteroepitaxial topological crystalline insulator thin films. *Nature Nano.* **10**, 849 (2015).

27. D. L. Smith, and C. Mailhiot, Proposal for strained type II superlattice infrared detectors. *J. Appl. Phys.* **62**, 2545-2548 (1987).

28. F. Fuchs, U. Weimer, W. Pletschen, J. Schmitz, E. Ahlswede, M. Walther, J. Wagner, and P. Koidl, High performance InAs/$Ga_{1-x}In_xSb$ superlattice infrared photodiodes. *Appl. Phys. Lett.* **71**, 3251-3253 (1997).

29. See Supplemental Material for wafer characterizations; more data about temperature and

magnetic field dependence.

30. T. L. Schmidt, S. Rachel, F. von Oppen, and L. I. Glazman. Inelastic Electron Backscattering in a Generic Helical Edge Channel. *Phys. Rev. Lett.* **108**, 156402 (2012).

31. A. Rod, T. L. Schmidt, and S. Rachel. Spin texture of generic helical edge states. *Phys. Rev. B* **91**, 245112 (2015).

32. J. Maciejko, X. L. Qi, and S. C. Zhang. Magnetoconductance of the quantum spin Hall state. *Phys. Rev. B* **82**, 155310 (2010).

Figure Captions

Fig. 1. Calculated band dispersions and wafer structures of the strained InAs/GaInSb QWs. (**a-c**) Calculated bulk band structure of the InAs/$Ga_{0.80}In_{0.20}Sb$ (8.7 nm/4 nm) QWs, InAs/$Ga_{0.75}In_{0.25}Sb$ (9 nm/4 nm) QWs, and InAs/$Ga_{0.68}In_{0.32}Sb$ (8 nm/4 nm) QWs, CB1, VB1 and CB2, VB2 are bands of different spin component. (**d**) Schematic drawing of band dispersion (both bulk states and edge states) in InAs/GaInSb QSHI system. (**e**) Wafer structures of the strained-layer InAs/$Ga_{0.75}In_{0.25}Sb$ QWs used for experiments. **(f)** Shown here as an example, a TEM photograph of the strained InAs/$Ga_{0.68}In_{0.32}Sb$ wafer; blue and red lines are guide for eyes.

Fig. 2. Transport data of bulk states from Corbino devices. G-V_{front} traces of a InAs/$Ga_{0.75}In_{0.25}Sb$ Corbino under different in-plane magnetic field at (**a**) V_{back} = 0 V and (**b**) V_{back} = 4 V. G-V_{front} traces under different perpendicular magnetic field at (**c**) V_{back} = 0 V and (**d**) V_{back} = 4 V. G-V_{front} traces under different in-plane magnetic field for (**e**) a InAs/$Ga_{0.80}In_{0.20}Sb$ Corbino and (**f**) a InAs/$Ga_{0.68}In_{0.32}Sb$ Corbino. (**g**) Arrhenius plots for InAs/GaSb QWs (open squares), InAs/$Ga_{0.80}In_{0.20}Sb$ QWs (open circles), InAs/$Ga_{0.75}In_{0.25}Sb$ QWs (filled diamonds), and InAs/$Ga_{0.68}In_{0.32}Sb$ QWs (filled circles). Energy gaps are deduced by fitting $G_{xx} \propto \exp(-\Delta/2k_BT)$, as shown by straight dash lines in the plot.

Fig. 3. Helical edge transport in strained-layer InAs/$Ga_{0.75}In_{0.25}Sb$ QWs. R_{xx}-V_{front} traces measured from (**a**) a 100 μm × 50 μm Hall bar device and (**b**) a 10 μm × 5 μm Hall bar device at T ~ 20 mK with V_{back} = 0 V, 1V, 2 V, 3 V, and 4 V. The edge characteristic length increases with decreasing V_{back}. The inset in (**a**) shows the λ_φ and the n_{cross} values at different backgate bias V_{back}.

Fig. 4. Helical edge conductance under magnetic field. (**a**) R_{xx}-V_{front} traces of a 3 μm × 1.5 μm Hall bar under different perpendicular magnetic field (V_{back} = 0 V). Inset in (**a**), the R_{CNP} values increase monotonically in the range of $B_\perp$ < 5 T, manifesting enhanced backscattering

processes in the helical edge under TRS breaking. (**b**) R_{xx}-V_{front} traces of the 3 μm × 1.5 μm Hall bar under different in-plane magnetic field. The plateau resistance values rise above the quantized value under $B_{//}$ because of TRS breaking. R_{xx}-V_{front} traces of the 100 μm × 50 μm Hall bar under different perpendicular magnetic field at (**c**) $V_{back} = 0$ V and (**d**) $V_{back} = 4$ V.

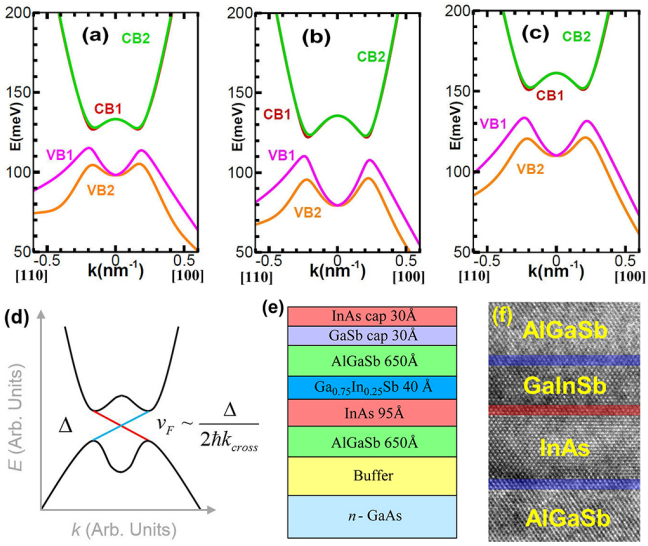
(a)
(b)
(c)
CB2
CB1
VB1
VB2
E(meV)
200
150
100
50
-0.5
0
0.5
k(nm-1)
[110]
[100]
(d)
E (Arb. Units)
k (Arb. Units)
Δ
$v_F \sim \frac{\Delta}{2\hbar k_{cross}}$
(e)
InAs cap 30Å
GaSb cap 30Å
AlGaSb 650Å
Ga0.75In0.25Sb 40 Å
InAs 95Å
AlGaSb 650Å
Buffer
n- GaAs
(f)
AlGaSb
GaInSb
InAs
AlGaSb

Figure 1

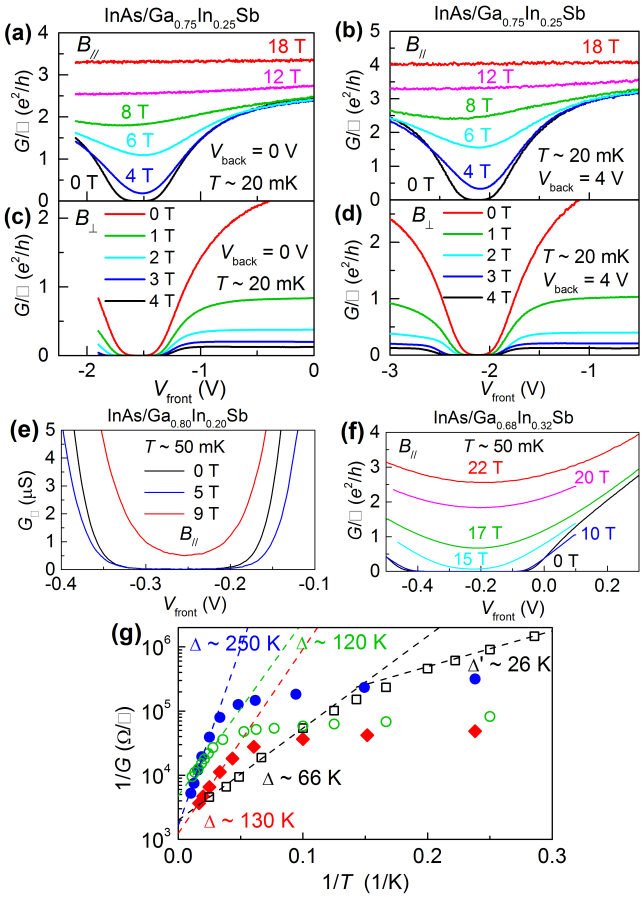
(a)
InAs/Ga0.75In0.25Sb
B//
18 T
12 T
8 T
6 T
4 T
0 T
Vback = 0 V
T ~ 20 mK
G/□ (e²/h)
(b)
InAs/Ga0.75In0.25Sb
B//
18 T
12 T
8 T
6 T
4 T
0 T
T ~ 20 mK
Vback = 4 V
G/□ (e²/h)
(c)
B⊥
0 T
1 T
2 T
3 T
4 T
Vback = 0 V
T ~ 20 mK
G/□ (e²/h)
Vfront (V)
(d)
B⊥
0 T
1 T
2 T
3 T
4 T
T ~ 20 mK
Vback = 4 V
G/□ (e²/h)
Vfront (V)
(e)
InAs/Ga0.80In0.20Sb
T ~ 50 mK
0 T
5 T
9 T
B//
G□ (μS)
Vfront (V)
(f)
InAs/Ga0.68In0.32Sb
B//
T ~ 50 mK
22 T
20 T
17 T
15 T
10 T
0 T
G/□ (e²/h)
Vfront (V)
(g)
Δ ~ 250 K
Δ ~ 120 K
Δ' ~ 26 K
Δ ~ 66 K
Δ ~ 130 K
1/G (Ω/□)
1/T (1/K)

Figure 2

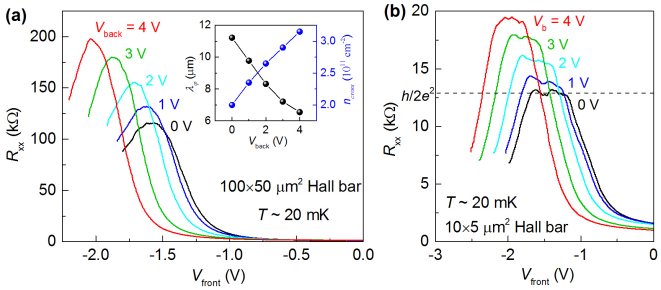
(a)
V_{back} = 4 V
3 V
2 V
1 V
0 V
R_{xx} (kΩ)
V_{front} (V)
100×50 μm² Hall bar
T ~ 20 mK
λ_c (μm)
n_{inner} (10^{11} cm^{-2})
V_{back} (V)
(b)
V_b = 4 V
3 V
2 V
1 V
0 V
h/2e²
R_{xx} (kΩ)
V_{front} (V)
T ~ 20 mK
10×5 μm² Hall bar

Figure 3

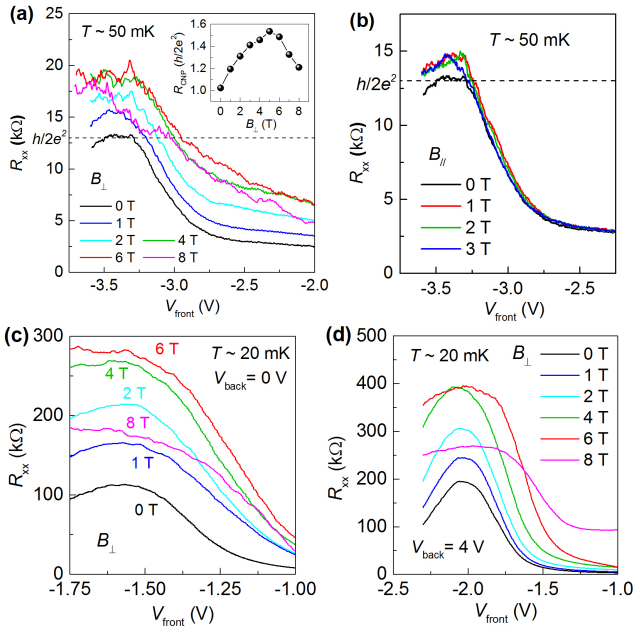
(a)
T ~ 50 mK
h/2e²
R_xx (kΩ)
B⊥
0 T
1 T
2 T
4 T
6 T
8 T
V_front (V)
R_CNP (h/2e²)
B⊥ (T)
(b)
T ~ 50 mK
h/2e²
R_xx (kΩ)
B//
0 T
1 T
2 T
3 T
V_front (V)
(c)
6 T
4 T
2 T
8 T
1 T
0 T
T ~ 20 mK
V_back = 0 V
R_xx (kΩ)
B⊥
V_front (V)
(d)
T ~ 20 mK
B⊥
0 T
1 T
2 T
4 T
6 T
8 T
V_back = 4 V
R_xx (kΩ)
V_front (V)

Figure 4